Eur. Phys. J. D (2016) 70: 3
DOI: 10.1140/epjd/e2015-60437-4

THE EUROPEAN
PHYSICAL JOURNAL D

Regular Article

Discharge processes and an electrical model of atmospheric pressure plasma jets in argon*

Zhi Fang[1], Tao Shao[2,3,a], Jing Yang[1], and Cheng Zhang[2,3]

[1] College of Electrical Engineering and Control Science, Nanjing Tech Technology, Nanjing 210009, P.R. China
[2] Institute of Electrical Engineering, Chinese Academy of Sciences, Beijing 100190, P.R. China
[3] Key Laboratory of Power Electronics and Electric Drive, Chinese Academy of Sciences, Beijing 100190, P.R. China

Received 29 July 2015 / Received in final form 13 September 2015

Abstract. In this paper, an atmospheric pressure plasma discharge in argon was generated using a needle-to-ring electrode configuration driven by a sinusoidal excitation voltage. The electric discharge processes and discharge characteristics were investigated by inspecting the voltage-current waveforms, Lissajous curves and lighting emission images. The change in discharge mode with applied voltage amplitude was studied and characterised, and three modes of corona discharge, dielectric barrier discharge (DBD) and jet discharge were identified, which appeared in turn with increasing applied voltage and can be distinguished clearly from the measured voltage-current waveforms, light-emission images and the changing gradient of discharge power with applied voltage. Based on the experimental results and discharge mechanism analysis, an equivalent electrical model and the corresponding equivalent circuit for characterising the whole discharge processes accurately was proposed, and the three discharge stages were characterised separately. A voltage-controlled current source (VCCS) associated with a resistance and a capacitance were used to represent the DBD stage, and the plasma plume and corona discharge were modelled by a variable capacitor in series with a variable resistor. Other factors that can influence the discharge, such as lead and stray capacitance values of the circuit, were also considered in the proposed model.

1 Introduction

The atmospheric pressure plasma jet (APPJ) has recently attracted great attention for their potential in many applications [1–3]. Working under gas flow conditions, the generated active species are not only confined to the electrode regime, and can be blown out of the reactor to form plasma with moderate energy density in open air. The APPJ has great flexibility, and imposes no limitations on the sizes of the objects to be treated. APPJ can treat the target from a distance and can treat large areas, especially for plasma treatment of three-dimensional complex materials, living objects and cells, thus facilitating its applications in surface treatment of materials, biomedicine and thin film deposition [4–6].

Various types of APPJ sources based on different geometric configurations have been developed, and the experimental and theoretical studies on their characteristics have been carried out, mainly focusing on understanding its formation mechanism [7–16]. For electrical characteristic analysis of the jet discharge, an equivalent electrical model is necessary and useful. From an electrical point of view, the jet system can be modelled by an equivalent electrical model, which complies with a power law [17–19]. Using this kind of model, the electrical parameters which cannot be measured directly from experiments can be obtained, and facilitating the study and analysis of the dynamic electrical behavior of the discharge, thus allowing us to study the discharge characteristics deeply and to determinate the optimal working conditions.

In recent years, several equivalent electrical models have been developed and used to characterise the discharge characteristics and behaviours of systems, in which the DBD plasma is modelled using either a temporally variable resistance, or a diode full bridge, or a voltage CCS combined with a temporally variable resistance [20–25]. Some researchers used the DBD-based model to study and analyse the electrical discharge characteristics of jet discharge [26–29]. However, there may be some inaccuracies and uncertainties for analysing the discharge characteristics of the APPJ by using the DBD based model. This is mainly due to discharge behaviours of the APPJ not being completely in agreement with DBD, which only generated plasma between the electrode regimes. Also, for some jet configurations, the discharge transits between several modes from breakdown to jet stage with increasing

---

* Contribution to the Topical Issue "Recent Breakthroughs in Microplasma Science and Technology", edited by Kurt Becker, Jose Lopez, David Staack, Klaus-Dieter Weltmann and Wei Dong Zhu.

[a] e-mail: `st@mail.iee.ac.cn`

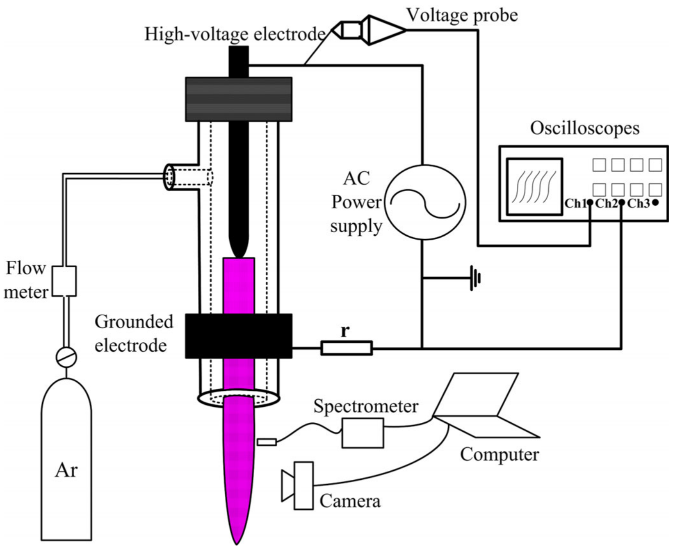

Fig. 1. Schematic diagram of the experimental set-up.

applied voltage [7,9,10,12,30–32], a model to characterise the whole discharge behaviour from discharge breakdown to the jet stage should be developed. Therefore, it is of importance to develop an equivalent electrical model to characterise the discharge, and thus to determine the electrical characteristics accurately, but there are yet few reports currently about the electrical models characterising jet discharge.

In this paper, a simple jet device with needle-to-ring electrodes was set up to generate the jet discharge in argon (Ar), and its discharge processes and discharge characteristics from breakdown with applied voltage were investigated. Based on the experimental results and discharge mechanism analysis, an equivalent electrical model and equivalent circuit for accurate analysis of the electrical characteristics of the discharge were proposed.

2 Experimental setup

A schematic illustration of the experimental setup is shown in Figure 1. The system consisted of a quartz tube, a high-voltage (HV) electrode and a grounded electrode. The inside and outside diameters of the quartz tube were 6 and 10 mm respectively, and the length is 180 mm. A copper rod with a diameter of 3 mm and length of 100 mm was inserted into the center of the quartz tube as a high voltage electrode. The copper rod was fastened by Teflon fitting at one end, and it had a sharp tip to reduce the breakdown voltage greatly, in order to ensure that the discharge would occur at relative low applied voltages. A 10 mm wide copper strip was wrapped on the outer surface of the quartz tube as a grounded electrode, and it was placed at a distance of 30 mm from the tip of the high-voltage electrode and 40 mm away from the edge of the quartz tube. High-purity argon (99.999%) was used as the working gas and was fed into the quartz tube, and its flow rate was measured and controlled by a mass flow controller, which was fixed at 4 L/min in our experiments. The discharge was powered by an AC sinusoidal HV power source with a frequency of 5−15 kHz and an adjustable peak voltage of 0−12 kV.

The voltage applied to the electrodes was measured via a Tektronix P6015A voltage probe, and the discharge current was measured using a 50 Ω non-inductive resistor (r) connected in series with the grounded electrode. The voltage and current waveforms were recorded by a digital oscilloscope (Tek TDS3054c (500 MHz, 5G S/s)). The discharge consumed power and transferred charge were obtained by using the measured voltage and current data. The light emission images of the plasma jets were taken by a Canon 400D digital camera mounted for taking pictures of the discharges from the side, with an exposure time of 1/30 s.

3 Discharge processes and characteristics

It was found that the generation and evolution of the discharge were sensitive to the applied voltage. When the peak applied voltage was raised above the breakdown threshold of 3.2 kV, discharge occured near the tip of the high-voltage electrode first, where a bright radiation spot was observed. With the increase in applied voltage, a thin cylindrical-shaped discharge channel started to extend downstream toward the grounded electrode, and no visible radiation between the front of the discharge channel and the grounded electrode was observed, as is seen in discharges 1−3 in Figure 2a. Then, as the peak applied voltage was increased to 3.8 kV, complete breakdown of a whole inter-electrode gap occurs, and a large bright plasma channel inside the quartz tube between the high-voltage electrode and grounded electrode were observed. With further increases in the applied voltage, the plasma channel was transmitted through the grounded electrode and extended along the quartz tube wall toward the open end of the quartz tube, as is seen in discharges 4−5 in Figure 2a. As the peak applied voltage approached to 5 kV, the plasma channel expanded out of the quartz tube outlet to form a plasma jet in ambient air, which can be seen in discharge 6 in Figure 2a. Figure 2b shows the evolution of the length of the plasma channel with the peak applied voltage. It can be seen that the length of the plasma jet can be increased to its maximum value of 3 cm when the peak applied voltage amplitude was increased from 5 kV to 8 kV. As the applied voltage was increased further, the plasma jet became brighter and remained stable, while its length became slightly shorter, as is seen in discharges 10−11 in Figure 2a. When the peak applied voltage reached 9.5 kV, the discharge became unstable, some plasma filaments appear along the quartz tube wall, between the high-voltage electrode and the grounded electrode. Therefore, it appears that 9.5 kV is the maximum voltage that our jet reactor can withstand, because no stable discharge could be obtained when the applied voltage is higher than this value.

The different operational regimes occurring with different applied voltages and the transitions between the regimes can also be identified by measuring the voltage

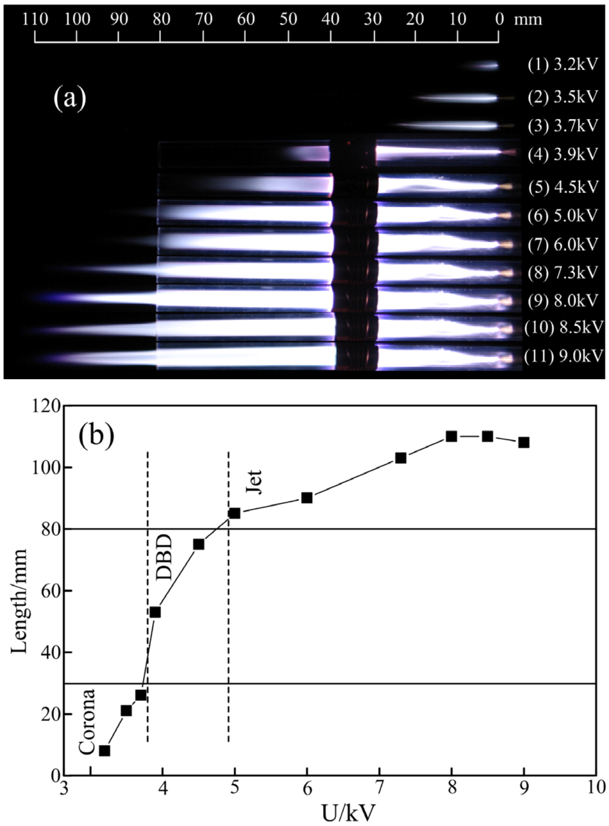

Fig. 2. Light-emission images (a) and a plot of the length of the plasma channel versus the peak applied voltage (b).

and current waveforms. It was evident that the current waveform underwent a sequence of distinct stages as the applied voltage was increased. Figure 3 shows the voltage and current waveforms measured under different peak applied voltages. It can be seen from Figures 3a and 3b that, when the peak applied voltage was below 3.8 kV, the current waveforms were characterised as a quasi-sinusoidal displacement current, superimposed with a significant number of discharge pulses in the form of micro-peaks. The peak current of the discharges was small, and did not exceed 1 mA. The discharge characteristics were similar to AC corona discharges in point-to-plane DBD reported in references [33–35]. When the peak applied voltage was increased above 3.9 kV, the discharge current changed abruptly both in waveform and in peak position. As shown in Figure 3c, there was only one dominant discharge current pulse per half cycle of the applied voltage, with each discharge being around a microsecond in duration. The discharge events were periodic, though the peak current in the positive half-cycle was not the same as that observed in the negative half-cycle. This is similar to the discharge behaviour observed in atmospheric pressure homogeneous DBD sustained between two parallel-plate electrodes [22–25]. The peak value of the positive current pulse was 25 mA with a duration of about 1.9 μs, and the peak values of the negative current pulse was 18 mA, which was slightly less than that of the positive current. Moreover, the duration of the negative current was slightly longer than that of the positive current, about 2.5 μs. The increase of peak applied voltage to 5 kV resulted in changes in the number and peak values of current pulses. There were two discharge current pulses both in the positive half cycle and in the negative half cycle in the waveform of the current. As can be seen from Figure 3d, there were two consecutive discharge current pulses with peak values of about 40 mA and 50 mA in the positive cycle for the applied voltage of 5 kV, and the durations of these current pulses were about 1.5 μs. Two current pulses with smaller peak values and longer durations were also observed in the negative cycle. In Figure 3d, the peak values of the two negative current pulses were 10 mA and 5 mA, and their durations were about 3 μs and 6 μs, respectively. Similar multiple current peaks in the current waveform in Figure 3d were also observed in atmospheric pressure DBD and reported in references [36–38], and it is regarded as an indication of pseudo-glow discharge, which may be due to the non-uniform surface charge distribution and density on the dielectric barrier surface and may also be due to the negative differential resistance of the cathode fall region. When the peak applied voltage was increased to larger than 5 kV, the discharge was observed to occur in jet mode. It can be seen from Figures 3e and 3f that an additional positive current pulse with a small peak intensity

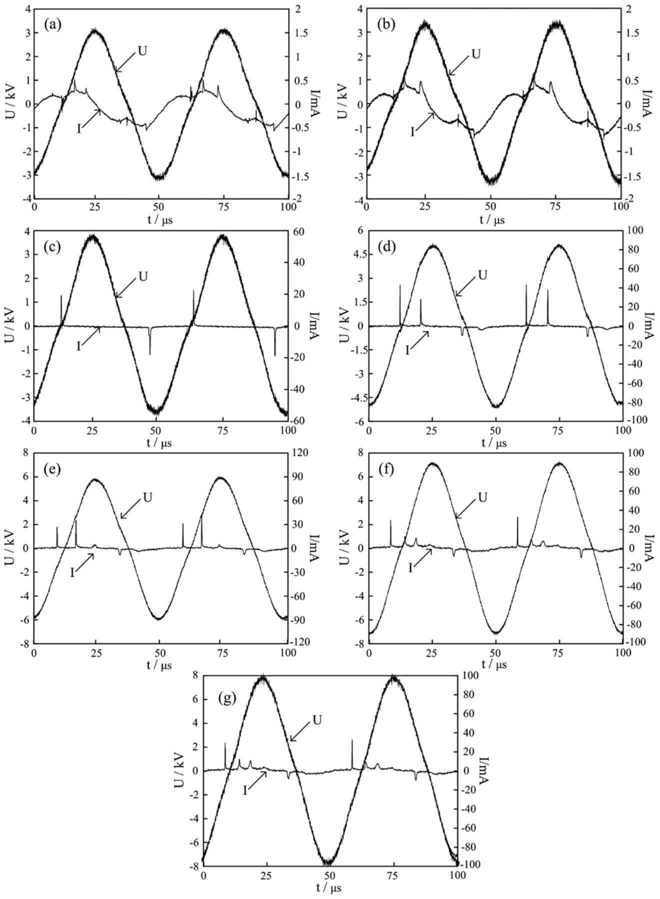

Fig. 3. Voltage and current waveforms measured at different applied voltages: (a) 3.2 kV (b) 3.7 kV (c) 3.9 kV (d) 5 kV (e) 6 kV (f) 7.3 kV (g) 8 kV.

and a longer duration appears, and the current curves in each case were characterised by two strong narrow positive pulses, followed by a weak broad positive pulses and two negative pulses. At further increased applied voltage, even four to five current pulses of positive polarities were observed, as is shown in Figure 3g. It was noted that the number of current pulses in the negative cycles did not change with the increase in applied voltage, and there were always two pulses appearing. The current waveform was not symmetrical for the positive and negative half-periods of the voltage, the negative half-period discharge was always much weaker than those observed within positive half-periods for all applied voltage.

The different discharge modes may result from different electric field distributions due to the arrangement of the electrodes, which is also asymmetrical, with the copper rod as the high voltage electrode, the copper strip as the grounded electrode and the quartz tube as the dielectric barrier. The asymmetrical electrode arrangement will cause a non-uniform electric field between the high-voltage electrode and the grounded electrode. When the AC voltage was applied to the electrodes, the electric field was formed inside the gas gap between the end of copper rod and the grounded electrode (copper ring). For a given applied voltage, the electric field at the vicinity near the copper rod would be higher than that around the downstream copper ring electrode. When the applied voltage was increased to the breakdown voltage (3.2 kV), the electric field near the copper rod reached the critical value for breakdown first, and the electric field strength was higher than the breakdown electric field for argon in this region, resulting in the formation of a corona-like discharge on the tip of the high-voltage electrode in argon gas. At this time, the electric field outside this region was not high enough to cause the breakdown in argon, therefore no discharge was generated in that region. With the increase in applied voltage, the region where the electric field strength was higher than the breakdown electric field extends towards the grounded electrode, so the corona discharge will extend towards the copper ring electrodes with the help of gas flow. When the applied voltage was sufficiently high (3.9 kV), the electric field in the region between the copper rod and the grounded electrode inside the quartz tube was higher than the breakdown electric field for argon, thus breakdown occurred also in the whole region. During this process, the charged particles (positive ions and electrons) will accumulate on the inner surface of the quartz tube to form surface charges. The surface charges accumulated formed an electric field which was in a reverse polarity with respect with applied electric field, and caused the total electrical field to decrease rapidly, thus quenching the breakdown and extinguishing the discharge. Due to the formation of the dielectric barrier, the electric field distribution was different from that observed in the corona discharge, and the electric field in the whole gap between the copper rod and the grounded electrode was high enough to form a glow-like discharge, and the discharge mode has been shown to evolve from the corona discharge to the glow-like DBD. With future increase in the applied peak voltage, the electric field in the region between the copper rod and the grounded electrode became stronger, and the ionisation also become stronger. More active species were generated in this region, so more of them were transferred to the down-stream region by the argon gas flow, leading to an extension of the plasma along the tube. When the peak applied voltage was larger than 5 kV, the plasma channel extended out of the quartz tube and intermixed with the surrounding air to form a plasma jet in ambient air. In this case, although the electric field outside the end of the quartz tube were not sufficient to ionise the gas molecules (nitrogen, water vapor and oxygen, etc.) in air, the electrons and metastable particles in the argon gas flow can ionise these gas molecules, leading to the propagation of the plasma jet in ambient air. In other words, the higher the applied peak voltage is, the more electrons and metastable particles depart into air from the quartz tube, so more of them can interact with gas molecules in air, and the longer is the jet length in air. When the peak applied voltage reached 8 kV, the jet length reached its maximum of 30 mm. This is mainly due to the fact that the Ar/air interface showed a gradual attenuation in the downstream direction. Hence the length of jet in the ambient air indicated the formation of the Ar/air interface via the inter-diffusion process. In the downstream direction, the farther away from the tube end, the more mixing of argon with air will occur, so it formed a saturation length that is related to the flow rate of the argon gas [12,13].

It should be noted that the distance separation between the high-voltage electrode and the grounded electrode can influence the discharge mode transitions. It was observed during our experiments that an increase in the electrode separation resulted in the change of the operation voltage range for these three modes. For example, at a larger electrode separation of 50 mm, the discharge started from corona discharge after breakdown at a lower applied voltage of 3.1 kV, while it transited to DBD and jet modes at higher applied voltages of 4.6 kV and 5.3 kV, respectively. This may be due to the fact that the electric field distribution was more non-uniform for larger electrode separation between the tip of copper rod and the copper ring grounded electrode, which meant that the tip of copper rod has higher electric field strength at certain applied voltages, and thus lower breakdown voltage. While the higher applied voltages for DBD and jet modes were due to thegreater electrode separation, which therefore needed higher applied voltage to achieve ionisation. Apart from the electrode separation, the flow rates of argon may also influence the discharge mode transitions, because changing of the flow rate may affect the ionisation of the discharge. As stated by other researchers, the influences of gas flow rate on characteristics of the jet plasma are complex [10,11,27,30]. In this paper, the experiments were conducted at a fixed gas flow rate of 4 L/min. It was expected that increasing the flow rate may cause an increase of the applied voltage required for achieving these three discharge modes, because more species will be brought to the downstream direction by the higher flow rate. Details on the influences of the flow rate on the discharge mode transitions need further investigation, and will be studied in our future work.

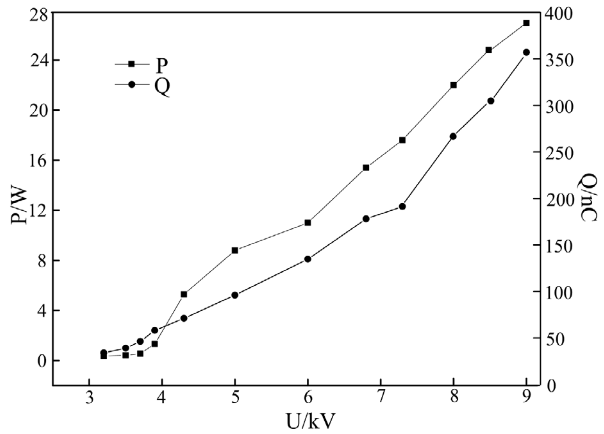

Fig. 4. Variation of the discharge power and charge transferred with applied voltage.

The discharge power was an important parameter to evaluate the efficiency of the discharge, and the evidence of discharge mode transitions can also be characterised by calculating the average discharge power. The average discharge power P can be calculated using the measured data of discharge voltage and current by the following formula:

$$P = \frac{1}{T}\int_0^T u\left(t\right) i\left(t\right) dt \qquad (1)$$

where T is the period of applied voltage, $u(t)$ and $i(t)$ are the instantaneous discharge voltage and discharge current measured, respectively. Figure 4 shows the characteristic curve of average discharge power dissipated versus the applied voltage amplitude. It is expected that the average discharge powers increase with the applied voltage, which is extremely consistent with the results shown in Figure 4. But the average discharge power was very non-linear, with the increase in the applied voltage, and the curve had a step shape with two transition points at applied voltages of 3.9 kV and 6 kV, respectively. When the applied voltage was increased from 3.2 kV to 3.9 kV, the average discharge power was observed to increase exponentially from 0.36 W to 0.55 W. When the applied voltage increased from 3.9 kV to 6 kV, a 1 kV increase in the applied voltage resulted in less than a 1 W increase in dissipated power; however, when the applied voltage increased from 6 kV to 9 kV, a 1 kV increase in the applied voltage yielded a 3 W increase in dissipated power. The non-linear relationship between the average discharge power and the applied voltage was a reflection of the discharge in different modes, because these two transitions observed in average discharge power versus applied voltage values agreed well with data obtained in Figure 2b. According to the experimental results, three modes were clearly discernable from measurements of dissipated power, and the gradient of each line gave an indication of the change in electrical conductivity of the discharge. Thus, we can conclude that the change of the ionisation process changed at the two critical applied voltage, due to a change in the electrical conductivity. The charge transferred Q versus the applied voltage amplitude is also shown in Figure 4, which was calculated using the measured data of discharge current using the following formula:

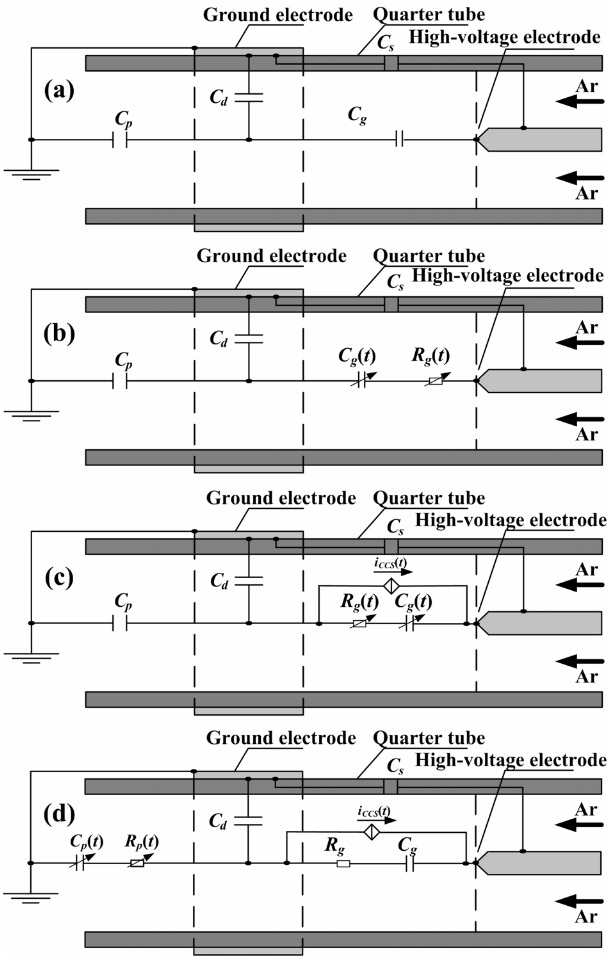

Fig. 5. Equivalent electrical models of the discharge (a) before breakdown, (b) during corona discharge, (c) during DBD, (d) during jet discharge.

$$Q = \int_0^T i(t)dt. \qquad (2)$$

It can be seen that the charge transferred increased more linearly with the increase in the applied voltage, indication an increase in ionisation of gas molecules in the discharge gap with applied voltage.

4 Electrical model

Based on the above mentioned experimental results and analysis, an equivalent electrical model shown in Figure 5 was proposed to represent the electrical behaviour of the discharge. If the applied voltage is not high enough to cause electric breakdown in the gap between electrodes, the discharge in the gas gap does not occur and the system is in the off state. In this stage, the equivalent electric model of the reactor can be considered as consisting of several capacitors connected in series, as shown in Figure 5a. The capacitor C_d represents the equivalent capacitance of the dielectric barrier (the quartz tube), and C_s represents the effect of parasitic capacitance between the high voltage electrode and the grounded electrode. The capacitors C_g and C_p are equivalent capacitances of the discharge gap and the plasma plume in surrounding air, respectively.

When the applied voltage exceeds the breakdown voltage, gas ionisation in the quartz tube occurs near the tip of the high-voltage electrode, and the discharge starts from the corona stage. In this stage, the equivalent electric model of the gas gap can be considered as consisting of an ohmic resistor representing the corona discharge, connected in series with the capacitance representing the non-breakdown gas gap, as shown in Figure 5b. It was known that the variation of the ionisation level after breakdown leads to the alteration of the value of the relative permittivity of the gas gap, thus modifying the equivalent capacitance and ohmic resistance of the gap, so the plasma impedance was represented by a variable $C_g(t)$ capcitor in series with a variable resistor $R_g(t)$, while $C_g(t)$ decreases and $R_g(t)$ increases with the applied voltage.

As the peak applied voltage is increased past a certain value, complete breakdown of whole inter-electrode gap inside the quartz tube between the high-voltage electrode and grounded electrode occurs, and the discharge mode transits from a corona discharge to the glow-like DBD. At this case, the discharge space in the dielectric tube corresponds to the discharge gap in a plane-plate DBD, so the equivalent electric model is similar to that for characterising DBD by other researchers. Our model was employed to represent the discharge phenomenon in the quartz tube, which is illustrated in Figure 5c. A voltage-controlled current source (VCCS) associated with a resistor and a capacitance has been used to represent the DBD discharge in the gas gap. In Figure 5c, a variable $C_g(t)$ value in series with a resistance $R_g(t)$ represent the plasma impedance, and their values change with applied voltage. Based on the phenomenology of DBD, the VCCS is based on the power law and represents the discharge current of the DBD plasma, and its current characteristic is defined by the applied voltage [23–25].

With further increases in applied voltage, the plasma channel transits the grounded electrode and expands out of the quartz tube outlet to form a plasma jet in ambient air. In this stage, the discharge in the inter-electrode gap inside the quartz tube between the high-voltage electrode and grounded electrode is still a DBD, so the equivalent electrical circuit model for the gap inside the quartz tube is the same with that in the previous DBD stage. Because the ionisation between the high-voltage electrode and grounded electrode is in the steady state, the constants C_g and R_g were used for characterising the plasma impedance of DBD in the tube. The propagation of plasma jet in ambient air leads to the alteration of the value of the relative permittivity of the air, thus modifying its equivalent resistance The plasma plume can be simulated by a variable $C_p(t)$ in series with a variable resistance $R_p(t)$. With the plume extending further in air with increasing applied voltage, $C_p(t)$ decreases and $R_p(t)$ increases, as shown in Figure 5d.

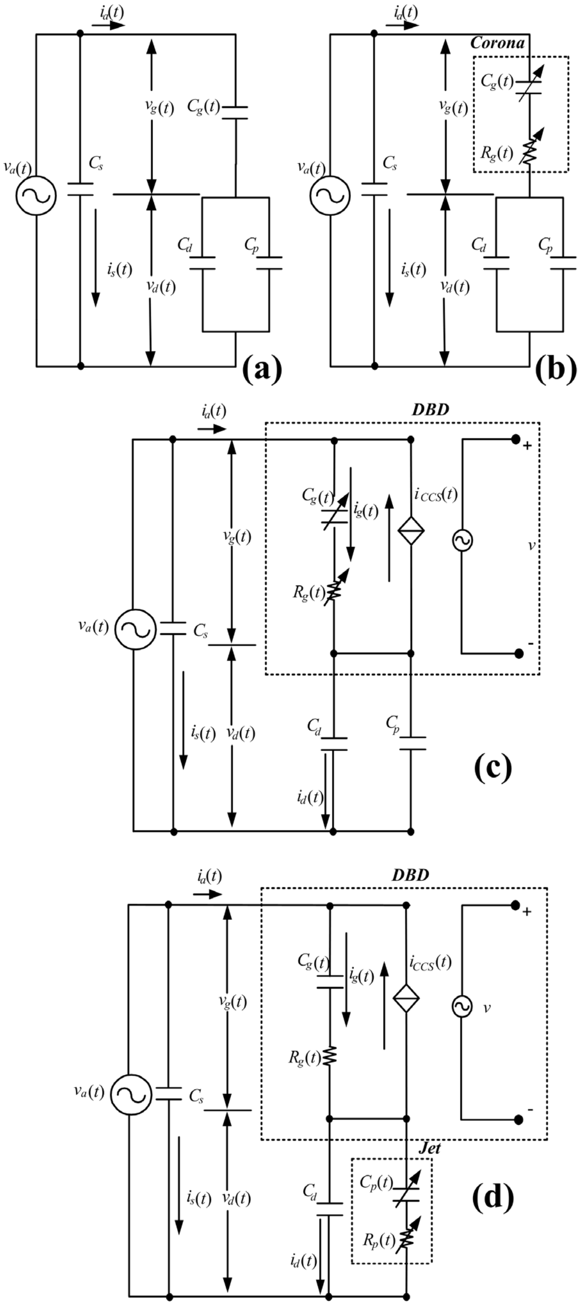

Fig. 6. Equivalent circuit diagrams of the discharge (a) before breakdown, (b) during corona discharge, (c) during DBD, (d) during jet discharge.

By considering the relationship of voltage and current, the electrical behaviour of the jet at different stages can be represented by an equivalent electric circuit model shown in Figure 6. In Figure 6, $v_a(t)$ is the applied voltage, $i_a(t)$ is the total external circuit current, $v_d(t)$ is the voltage across the dielectric barriers, $v_g(t)$ is the voltage across the gas gap, $i_g(t)$ is the displacement current in the gas gap, $i_d(t)$ is the displacement current in the dielectric barrier,

$i_{\mathrm{CCS}}(t)$ is the current voltage-controlled source that represents the discharge current in the gas gap, and $i_s(t)$ is the displacement current through C_S.

The equivalent electrical model developed in Figure 6 is relatively convenient and simple, and it reveals the interaction between the power supply and the plasma reactor, and can be used as a useful diagnostic tool for studying the dynamic electrical behavior of the reactor. For a given configuration and set of operation conditions, the values of C_g, C_d and C_p can be calculated from the geometry of the reactor. The values of $C_S$can be deduced by using the capacitance values measured when no discharge activity is observed. The values of the other electric components ($C_g(t)$, $R_g(t)$ and $C_p(t)$) for representing the variable plasma impedance at different discharge stage can be determined by running the simulation using the electrical model and comparing the results with experimental ones, until a very high correlation between the experimental and theoretical results was found. Using this model, the dynamic behaviour of the discharge parameters (such as gas gap voltage, discharge current, discharge consumed power, and transported charges) under different operation conditions, which are not measurable in the real process, can be obtained; hence, it considerably facilitates the study and analysis of the dynamic electrical behaviour of discharge, thus allowing not only the determination of the optimal working condition in the reactors but also designing of appropriate HV power sources for jet applications. Also, the flexibility of the model enables one to study the electrical characteristics of homogeneous DBD in other gases and discharge conditions, provided that several appropriate parameters were adjusted for each case. For the discharges in other gases such as helium and neon, the values of C_g, C_d and C_p in Figure 6 should be calculated using the permittivity of applied gas, and the values of $\mathrm{C_S}$ and operation voltage ranges of the three modes for specific gas should be determined from experimental measurement data for each gas used, then the same models described in this paper for argon can be used. For the discharges in other conditions such as different electrode separations, the values of C_g, C_d and C_p should be calculated using the geometry of the jet cell, and the operational voltage ranges of the three modes for specific electrode separation should be determined empirically. For the discharges in different flow rates, except for the above adjustments for other gases and the electrode separation, the operation voltage ranges of the three modes for different gas flow rates should also be determined empirically. Our further work will involve using this model to simulate the voltage and current, and to study on the electrical characteristics of APPJ under different operating conditions.

5 Summary

The discharge processes of an atmospheric pressure argon plasma in a rod-to-ring electrode configuration with varying applied voltage were studied by electrical and optical diagnosis. The discharge started from corona discharge, after breakdown at an applied voltage of 3.2 kV, and it transited to DBD mode at 3.8 kV, then to jet mode in ambient air when the voltage was further increased to 5 kV. The three stages could be distinguished clearly by their voltage-current waveforms, light-emission images and the changing tendency of the average discharge power with applied voltage. The corona discharge has a peak that is current less than 1 mA, and the discharges were tens of mA for both the DBD and jet modes. The average discharge power increased non- lineally with applied voltage, and the two transition points for the gradient of the discharge power-applied voltage curve agreed well with voltage values for the discharge mode transition. The different discharge modes resulted from the non-uniform electric field between the high-voltage electrode and the grounded electrode, the electric field near the copper rod firstly reached the critical value for breakdown to occur. Based on the experimental studies and analysis, the equivalent electrical model for characterising the discharge accurately was proposed, with the three discharge stages being characterised separately. The plasma plume and corona discharge were represented by a variable capacitor in series with a variable resistor, and a voltage-controlled current source (VCCS) associated to a resistance and a capacitance has been used to represent the DBD discharge between the two electrodes. Other factors that can influence the discharge, such as stray capacitance values of the circuit, were also considered in the proposed model. By considering the relationship between voltage and current, the equivalent circuit for characterising the discharge is deduced. This model can simulate of the voltage and current within a discharge, and it will be conducted in our future work. It can also be used to study and analyse of the dynamic electrical behaviour of discharge, thus facilitating not only the determination of the optimal working condition in the reactors, but also aid in the designing of appropriate HV power sources for jet applications.

This work was supported by the National Natural Science Foundation of China under Contracts Nos. 51377075 and 51222701, the Natural Science Foundation of Jiangsu Province China under Contract No. BK20131412, the Natural Science Fund for Colleges and Universities in Jiangsu Province under Grant No. 14KJB470004, the “Qing Lan Project” in Jiangsu Province of China, and the National Basic Research Program of China under Contract No. 2014CB239505-3.

References

1. L. Bárdos, L. Baránková, Thin Solid Films **318**, 6705 (2010)
2. K.D. Weltmann, E. Kindel, T. von Woedtke, M.L. Hähnel, M. Stieber, R. Brandenburg, Pure Appl. Chem. **82**, 1223 (2010)
3. M. Laroussi, T. Akan, Plasma Process. Polym. **4**, 777 (2007)
4. F. Iza, G.J. Kim, S.M. Lee, J.K. Lee, J.L. Walsh, Y.T. Zhang, M.G. Kong, Plasma Process. Polym. **5**, 322 (2008)
5. G. Fridman, G. Friedman, A. Gutsol, A.B. Shekhter, V.N. Vasilets, A. Fridman, Plasma Process. Polym. **5**, 503 (2008)

6. D. Pappas, J. Vac. Sci. Technol. A **29**, 020801 (2011)
7. X. Lu, M. Laroussi, V. Puech, Plasma Sources Sci. Technol. **21**, 034005 (2012)
8. H.W. Lee, G.Y. Park, Y.S. Seo, Y.H. Im, S.B. Shim, H.J. Lee, J. Phys. D **44**, 053001 (2011)
9. J.L. Walsh, F. Iza, N.B. Janson, V.J. Law, M.G. Kong, J. Phys. D **43**, 75201 (2010)
10. S.J. Kim, T.H. Chung, S.H. Bae, Thin Solid Films **517**, **14**, 4251 (2009)
11. M.Y. Qian, C.S. Ren, D.Z. Wang, Q.Q. Fan, Q.Y. Nie, IEEE Trans. Plasma Sci. **40**, 1134 (2012)
12. Y. Xian, X. Lu, Z. Tang, Q. Xiong, W. Gong, D. Liu, Z. Jiang, Y. Pan, J. Appl. Phys. **107**, 063308 (2010)
13. S.J. Kim, T.H. Chung, S.H. Bae, Thin Solid Films **517,** 4251 (2009)
14. A.Y. Nikiforov, A. Sarani, C. Leys, Plasma Sources Sci. Technol. **20,** 015014 (2011)
15. A.A. Mohamed, K.C. Woo, H.W. Lee, J.K. Lee, K.T. Kim, IEEE Trans. Plasma Sci. **38**, 2954 (2010)
16. A. Kuwabara, S. Kuroda, H. Kubota, Plasma Chem. Plasma Process. **28**, 263 (2008)
17. S. Haslinger, J. Laimer, H. Stori, Vacuum **82**, 142 (2008)
18. C. Monge-Dauge, F. Clement, P. Svarnas, IEEE Trans. Plasma Sci. **40**, 2254 (2012)
19. S.Z. Li, W.T. Huang, J.L. Zhang, D.Z. Wang, Appl. Phys. Lett. **94**, 111501 (2009)
20. O. Koudriavtsev, S. Wang, Y. Konishi, M. Nakaoka, IEEE Trans. Ind. Appl. **38**, 369 (2002)
21. S. Liu, M. Neiger, J. Phys. D **36**, 3144 (2003)
22. N. Naudé, J.-P. Cambronne, N. Gherardi, F. Massines, J. Phys. D **38**, 530 (2005)
23. R. Valdivia-Barrientos, J. Pacheco-Sotel, M. Pacheco-Pacheco, J.S. Benítez-Read, R. López-Callejas, Plasma Sources Sci. Technol. **15**, 237 (2006)
24. U.N. Pal, P. Gulati, N. Kumar, R. Prakash, V. Srivastava, IEEE Trans. Plasma Sci. **40**, 1356 (2012)
25. Z. Fang, S. Ji, J. Pan, T. Shao, C. Zhang, IEEE Trans. Plasma Sci. **40**, 883 (2012)
26. Y. Xian, X. Lu, Z. Tang, Q. Xiong, W. Gong, D. Liu, Z. Jiang, Y. Pan, J. Appl. Phys. **107**, 063308 (2010)
27. S.Z. Li, J.P. Lim, H.S. Uhm, Phys. Lett. A **360**, 304 (2006)
28. H. Akamatsu, K. Ichikawa, Surf. Coat. Technol. **206**, 920 (2011)
29. S. Coulombe, V. Léveillé, S. Yonson, R.L. Leask, Pure Appl. Chem. **78**, 1147 (2006)
30. Z. Hao, S. Ji, A. Qiu, IEEE Trans. Plasma Sci. **40**, 2822 (2012)
31. Y. Hong, N. Lu, J. Pan, J. Li, Y. Wu, Thin Solid Films **531**, 408 (2013)
32. Y. Hong, N. Lu, J. Pan, J. Li, Y. Wu, K.F. Shang, J. Electrostat. **71**, 93 (2013)
33. I. Radu, R. Bartnikas, M.R. Wertheimer, J. Phys. D **36**, 1284 (2003)
34. Yu. S. Akishev, A.V. Demyanov, V.B. Karalnik, A.E. Monich, N.I. Trushkin, Plasma Phys. Rep. **29**, 82 (2003)
35. M. Abdel-Salam, A. Hashem, A. Yehia, A. Mizuno, A. Turky, A. Gabr, J. Phys. D **36**, 252 (2003)
36. Yu. S. Akishev, A.V. Demyanov, V.B. Karalnik, M.V. Pankin, N.I. Trushkin, Plasma Phys. Rep. **27**, 164 (2001)
37. X. Tu, B. Verheyde, Corthals, S. Paulussen, B.F. Sels, Phys. Plasmas **18**, 080702 (2011)
38. L. Mangolini, K. Orlov, U. Kortshagen, J. Heberlein, U. Kogelschatz, Appl. Phys. Lett. **80**, 1722 (2002)